RESEARCH ARTICLE SUMMARY

DNA NANOTECHNOLOGY

A cargo-sorting DNA robot

Anupama J. Thubagere, Wei Li, Robert F. Johnson, Zibo Chen, Shayan Doroudi, Yae Lim Lee, Gregory Izatt, Sarah Wittman, Niranjan Srinivas, Damien Woods, Erik Winfree, Lulu Qian*

INTRODUCTION: Since the 1980s, the design and synthesis of molecular machines has been identified as a grand challenge for molecular engineering. Robots are an important type of molecular machine that automatically carry out complex nanomechanical tasks. DNA molecules are excellent materials for building molecular robots, because their geometric, thermodynamic, and kinetic properties are well understood and highly programmable. So far, the development of DNA robots has been limited to simple functions. Most DNA robots were designed to perform a single function: walking in a controlled direction. A few demonstrations included a second function combined with walking (for example, picking up nanoparticles or choosing a path at a junction). However, these relatively more complex functions were also more difficult to control, and the complexity of the tasks was limited to what the robot can perform within 3 to 12 steps. In addition, each robot design was tailored for a specific task, complicating efforts to develop new robots that perform new tasks by combining functions and mechanisms.

RATIONALE: The design and synthesis of molecular robots presents two critical challenges, those of modularity and algorithm simplicity, which have been transformative in other areas of molecular engineering. For example, simple and modular building blocks have been used for scaling up molecular information processing with DNA circuits. As in DNA circuits, simple building blocks for DNA robots could enable more complex nanomechanical tasks, whereas modularity could allow diverse new functions performed by robots using the same set of building blocks.

RESULTS: We demonstrate a DNA robot that performs a nanomechanical task substantially more sophisticated than previous work. We developed a simple algorithm and three modular building blocks for a DNA robot that performs autonomous cargo sorting. The robot explores a two-dimensional testing ground on the surface of DNA origami, picks up multiple cargos of two types that are initially at unordered locations, and delivers each type to a specified destination until all cargo molecules are sorted into two distinct piles. The robot is designed to perform a random walk without any energy supply. Exploiting this feature, a single robot can repeatedly sort multiple cargos. Localization on DNA origami allows for distinct cargo-sorting tasks to take place simultaneously in one test tube or for multiple robots to collectively perform the same task. On average, our robot performed approximately 300 steps while sorting the cargos. The number of steps is one to two magnitudes larger than the previously demonstrated DNA robots performing additional tasks while walking. Using exactly the same robot design, the system could be generalized to multiple types of cargos with arbitrary initial distributions, and to many instances of distinct tasks in parallel, whereas each task can be assigned a distinct number of robots depending on the difficulty of the task.

CONCLUSION: Using aptamers, antibodies, or direct conjugation, small chemicals, metal nanoparticles, and proteins could be transported as cargo molecules so that the cargo-sorting DNA robots could have potential applications in autonomous chemical synthesis, in manufacturing responsive molecular devices, and in programmable therapeutics. The building blocks developed in this work could also be used for diverse functions other than cargo sorting. For example, inspired by ant foraging, adding a new building block for leaving pheromone-like signals on a path, DNA robots could be programmed to find the shortest path and efficiently transport cargo molecules. With simple communication between the robots, they could perform even more sophisticated tasks. With more effort in developing modular and collective molecular robots, and with simple and systematic approaches, molecular robots could eventually be easily programmed like macroscopic robots, but working in microscopic environments. ∎
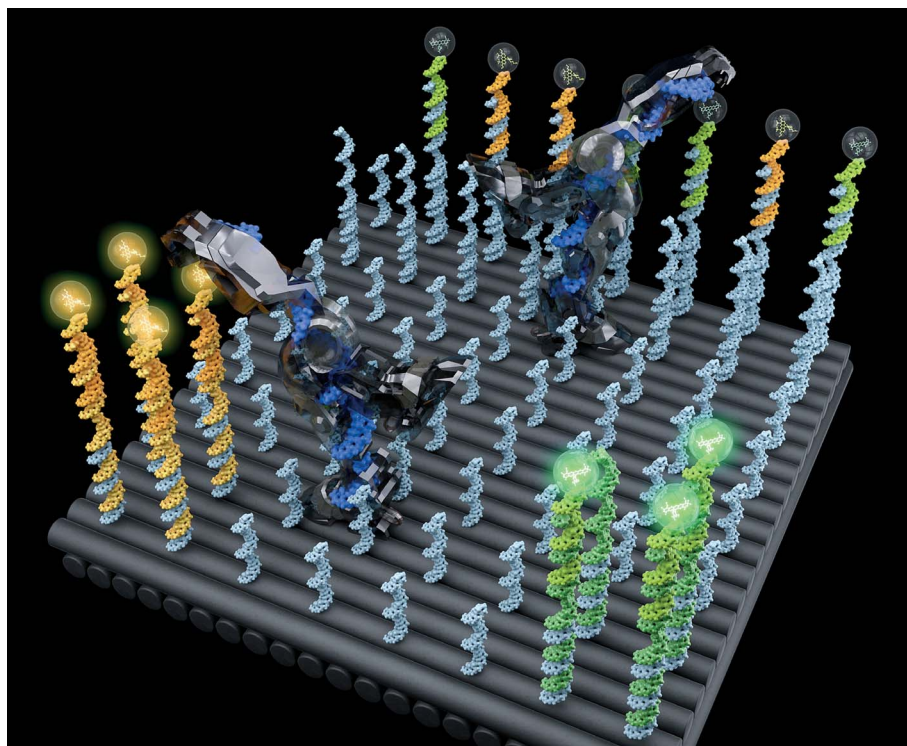
Conceptual illustration of two DNA robots. The robots are collectively performing a cargo-sorting task on a DNA origami surface, transporting fluorescent molecules with different colors from initially unordered locations to separated destinations. Considerable artistic license has been taken.

DNA NANOTECHNOLOGY

A cargo-sorting DNA robot

Anupama J. Thubagere,[1] Wei Li,[1] Robert F. Johnson,[1] Zibo Chen,[1] Shayan Doroudi,[2]
Yae Lim Lee,[3] Gregory Izatt,[2,4] Sarah Wittman,[2] Niranjan Srinivas,[4] Damien Woods,[2]*
Erik Winfree,[1,2,4] Lulu Qian[1,2]†

Two critical challenges in the design and synthesis of molecular robots are modularity and
algorithm simplicity. We demonstrate three modular building blocks for a DNA robot that
performs cargo sorting at the molecular level. A simple algorithm encoding recognition between
cargos and their destinations allows for a simple robot design: a single-stranded DNA with
one leg and two foot domains for walking, and one arm and one hand domain for picking up and
dropping off cargos. The robot explores a two-dimensional testing ground on the surface of
DNA origami, picks up multiple cargos of two types that are initially at unordered locations, and
delivers them to specified destinations until all molecules are sorted into two distinct piles.
The robot is designed to perform a random walk without any energy supply. Exploiting this
feature, a single robot can repeatedly sort multiple cargos. Localization on DNA origami allows
for distinct cargo-sorting tasks to take place simultaneously in one test tube or for multiple
robots to collectively perform the same task.

M olecular machines that perform mechanical tasks are key functional components in all biological organisms. The design of programmable molecular robots that automatically carry out complex nanomechanical tasks, while interacting with their environments, presents two critical challenges in molecular engineering, those of modularity and algorithm simplicity.

The importance of modularity in electromechanical robots was first established in the 1970s (*1*). Modular robots can be adaptive, be amenable to self-repair, and perform a variety of tasks using just one set of components. For example, long-term space missions need robots that handle unforeseen situations during autonomous operations. Modularity is also important for molecular robots not only because there are numerous unforeseen situations in the biochemical environments in which they operate but also because substantial effort is required to develop new molecular robots tailored for specific new tasks. Recent developments in protein motors have shown the potential of modularity, for example, in creating new functions from known protein motifs (*2*, *3*).

Complex individual molecules are difficult to create and are even more difficult to endow with precisely controlled dynamical and mechanical properties. Thus, the simpler the algorithm, the more likely that it can be performed by simple molecules, and the simpler the molecular im-

plementation, the more likely the experimental demonstration will be successful. Simple algorithms can give rise to sophisticated functions, including Turing-universal computation (*4*). Studies of the behavior of social insects, such as ants and termites, have shown that surprisingly complex tasks can be performed by individuals with limited capabilities. Their behavior has inspired simple but powerful solutions to complex engineering challenges (*5*).

We now show that a simple algorithm enables the demonstration of a simple DNA robot performing complex cargo-sorting tasks on two-dimensional (2D) DNA origami (*6*) surfaces. The system uses three building blocks that are composable with each other and could be used for diverse functions other than cargo sorting.

Framework

Chemically synthesized small DNA molecules are natural building blocks for modular designs because a continuous segment of nucleotides can serve as an independent domain in hybridization (*7*) or strand displacement (*8*). Various mechanical devices made of DNA molecules have been designed and synthesized, including tweezers (*8*), a polymerization motor (*9*), and a rotary apparatus (*10*). DNA robots have been developed from nonautonomous (*11*, *12*) to autonomous (*13–16*) and from walking in a controlled direction (*17*, *18*) to making a turn (*19*), choosing a branch (*20*), picking up cargos (*21*), and walking on a microparticle surface (*22*).

We chose cargo sorting as an example task because the function is substantially more complex than what previous DNA robots were capable of performing, is algorithmically interesting, and plays a crucial role in many biological and engineered systems. For example, in neurons, distinct proteins, including neurotransmitter

receptors and ion channels, are synthesized at the same place in the cell body but delivered to different places in axons and dendrites (*23*). In ant colonies, workers sort their brood by clustering eggs and microlarvae at the center area and by pushing the larger larvae farther from the center in order of increasing size (*24*). Sorting is also one of the most fundamental techniques in computer science and engineering. A variety of sorting algorithms have been developed to optimize data processing (*25*). Arranging items in order, whether they are information or physical objects, makes it easier to accomplish many other tasks, including searching and comparing.

There are two main reasons to develop a robot that performs cargo sorting on the surface of DNA origami, instead of just letting the cargo molecules diffuse to their destinations in solution. First, the initial and final geometrical locations of cargos could be an integral part of a sorting task. For example, if dendritic membrane proteins are incorrectly delivered to the axon of a neuron, they can be incorporated into the axonal membrane and cause the axon to take on dendritic properties, thus losing its identity (*23*). Second, the geometrical separation of individual robots working on their own testing grounds makes it possible for distinct cargo-sorting tasks to take place in parallel and for multiple robots to collectively perform the same task. Localization on DNA origami surfaces provides some of the same benefits as compartmentalization in biology, where membranes allow individual cells to perform distinct local functions in parallel and communication between cells then gives rise to complex global functions within an organism (*26*).

Algorithm

The task of cargo sorting is defined as follows: Initially, two or more types of molecules with multiple molecules per type are placed in a finite-size 2D space. The locations of these molecules can be arbitrary. A robot should be able to search the entire space, pick up any type of molecule, and deliver each type to a specified destination until all molecules are sorted into distinct piles (Fig. 1A).

If we were not limited by the capability of individual molecules, the following straightforward and efficient algorithm would be desirable. The robot systematically explores the relevant area. If it bumps into a cargo, the robot will pick it up, recognize the cargo type, choose a path that is directed to the specified destination for this cargo type, and drop it off at the destination. Then, the robot will repeat the process until all cargos are sorted. To implement this algorithm, the robot will need to have a memory for where it has been, the ability to recognize various types of cargos, and a procedure for choosing distinct paths directed to various destinations. These functions require the molecules composing the robot to be capable of information processing, and a cargo-sorting task with more types of cargos will require a more complex information processing circuit built into the robot.

[1]Bioengineering, California Institute of Technology, Pasadena, CA 91125, USA. [2]Computer Science, California Institute of Technology, Pasadena, CA 91125, USA. [3]Electrical Engineering, California Institute of Technology, Pasadena, CA 91125, USA. [4]Computation and Neural Systems, California Institute of Technology, Pasadena, CA 91125, USA.
*Present address: Inria, Paris, France. †Corresponding author. Email: luluqian@caltech.edu
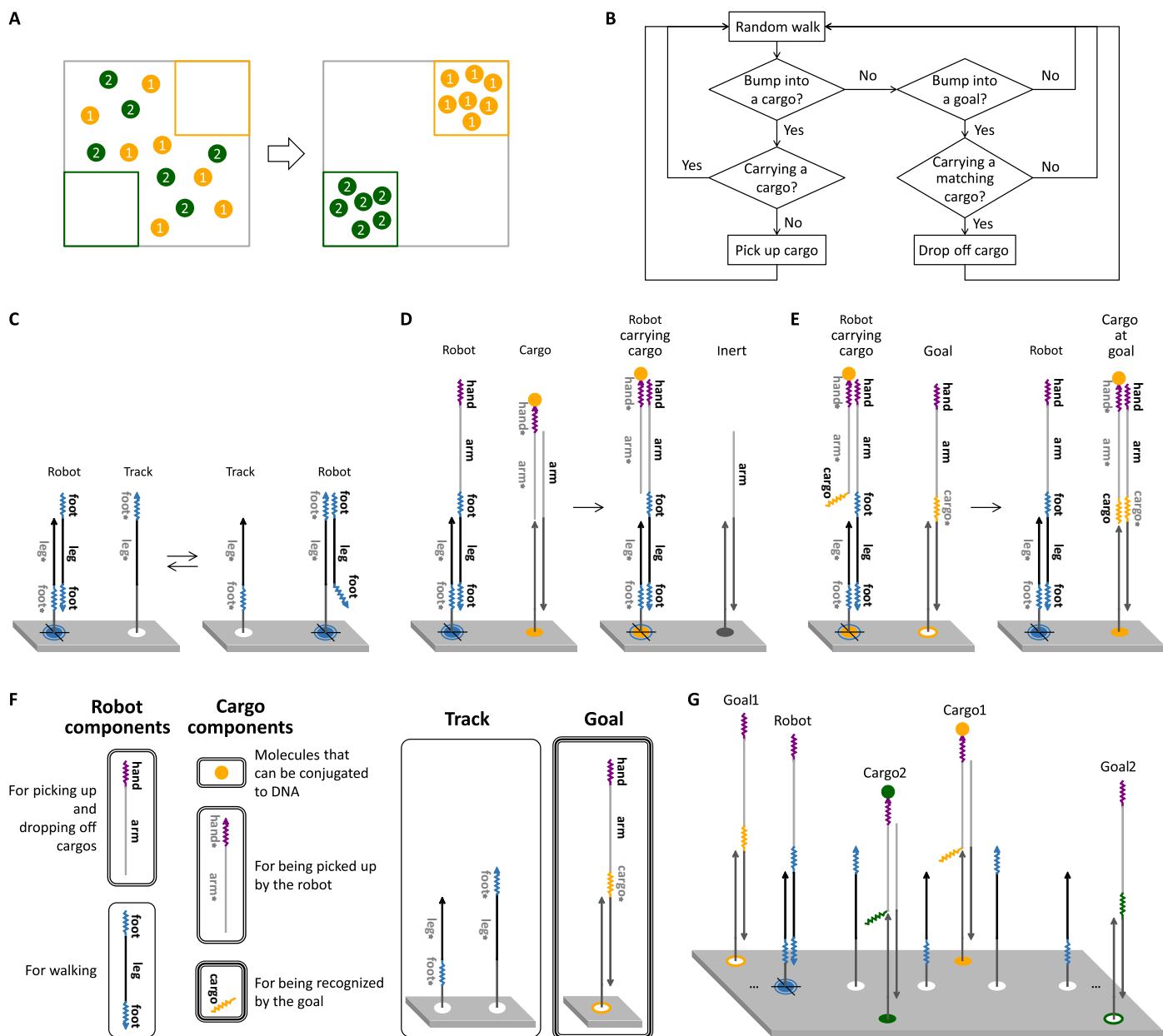
Fig. 1. The cargo-sorting algorithm. (**A**) Schematic diagram of sorting arbitrarily distributed molecules into distinct piles at specified destinations. (**B**) Flowchart of a simple cargo-sorting algorithm. In the molecular implementation, choices for picking up and dropping off cargos are not always taken as designed—the robot may instead return to random walking with a small probability. Mechanism of the three building blocks for the (**C**) random walk, (**D**) cargo pickup, and (**E**) cargo drop-off. (**F**) Composability of the three building blocks. Three types of outlines highlight the components used in the three building blocks. (**G**) Implementation for sorting multiple types of cargos. Squiggled lines indicate short toehold domains and straight lines indicate long branch migration domains in DNA strands, with arrowheads marking their 3′ ends.

To allow a practical molecular implementation, we developed a much simpler algorithm (Fig. 1B), similar to the ant-inspired sorting algorithms used in collective robotics (*27*, *28*), in which the robot performs a random walk. If it bumps into a cargo, the robot will pick it up and continue with the random walk. If it bumps into a goal that is the specified destination of the cargo, the robot will drop it off. Then, the robot will repeat the process until all cargos are sorted. To implement this algorithm, the robot will only need to be capable of random walking,

picking up cargos, and dropping them off. The robot will recognize neither the type of cargo nor the type of destination. The goal will recognize a matching cargo and force the robot to drop it off. The complexity of the robot molecule will remain the same with an increasing number of cargo types. The complexity of the cargo and goal molecules will also remain the same, so long as the recognition between each type of cargo and goal has sufficient specificity.

Using DNA strand displacement reactions (*8*, *29*, *30*), we developed three modular building

blocks—for the random walk, the cargo pickup, and the cargo drop-off—to implement the simple cargo-sorting algorithm. To perform a random walk on a track, a single-stranded DNA robot is designed with two foot domains of 6 nucleotides each and one leg domain of 15 nucleotides (Fig. 1C). The track is composed of a number of single-stranded extensions on a 2D DNA origami (*6*) surface. Each track strand binds to the robot through a complementary foot and leg domain, leaving another foot domain of the robot free. The robot moves from one location on the track

to another through a reversible strand displacement reaction. The free foot domain of the robot first binds to the complementary foot domain of a neighboring track strand. Branch migration occurs when the complementary leg domains of the two adjacent track strands compete with each other for binding to the leg domain of the robot. When branch migration proceeds to the end of the leg domain, the previously bound foot domain of the robot will disassociate, resulting in the robot moving one step away from the previous location. There are two types of track strands arranged in a checkerboard pattern: Each binds to one foot domain either at the 3′ end or at the 5′ end of the robot. The robot should be able to take a step from any location on the track to any neighboring location without a bias, because the track strands at all neighboring locations are identical and equidistant.

Extending the single-stranded DNA robot with an arm and hand domain allows for cargo pickup (Fig. 1D). A cargo molecule can be a DNA strand, referred to as the cargo strand, or any molecule conjugated to the 3′ end of the cargo strand. Here, we use a fluorophore or the DNA strand itself as a cargo. The cargo strand has a complementary hand and arm domain. It is initially bound to the DNA origami surface while leaving the complementary hand domain free. If the robot is at a neighboring location of the cargo strand, it will pick up the cargo through an irreversible strand displacement reaction. The reaction is initiated by binding of the hand domain and completed by branch migration within the arm domain. Because both the hand and arm domains of the robot will become double-stranded at the end of the reaction, the robot cannot pick up another cargo while carrying a cargo. After the cargo has been picked up, the original location of the cargo is now considered as inert. This change of state occurs because a single-stranded arm domain alone, without a hand domain, cannot interact with any other molecules in the system. The foot and leg domains function independently of the hand and arm domains, and thus, the robot should be able to perform a random walk whether or not it is carrying a cargo.

Adding a cargo domain to the cargo strand allows for drop-off (Fig. 1E). A goal strand on the DNA origami surface is designed to have a hand, arm, and complementary cargo domain. The robot drops off the cargo through an irreversible strand displacement reaction, similar to cargo pickup. The reaction is initiated by binding of the cargo domain between the cargo and goal strands, and completed by branch migration within the arm and hand domains. In this way, the goal actively grabs the cargo from the robot. Once the cargo is dropped off, all domains in the cargo and goal complex are double-stranded, and thus, no further reactions could take place at the destination. Without a cargo, the robot is now free to explore other locations on the origami surface and pick up another cargo.

The DNA strands and the domains in the strands used in each of the three building blocks

are directly composable with each other (Fig. 1F). Thus, the mechanism of cargo sorting simply combines the mechanisms for random walking, for picking up cargos, and for dropping off cargos. To sort multiple types of cargos, we just need to make sure that each type of cargo and goal strand has a unique cargo domain (Fig. 1G).

The random walk

To gain a quantitative understanding of the random walk building block and compare it with the basic aspects of random-walk theory (*31*), we started the experimental demonstration with a linear track on a DNA origami surface (Fig. 2A). To reduce the possibility of the robot getting stuck at any location on the track if a track strand is missing, we designed the track to be three sites wide. To identify the time required for the robot to travel a certain distance, we used a specified start and destination. The robot is designed to wait at the start location until a trigger signal is introduced and to stop walking once it reaches the destination.

Although the hand and arm domains are not needed for walking, we used them to design an inhibitor strand that forces the robot to wait at the start location (Fig. 2B). In addition to the complementary hand and arm domains that keep it stably bound to the robot, the inhibitor strand has a complementary foot domain to cover up the robot's foot that is not bound to the track. Thus, the robot cannot start walking without a free foot. The inhibitor strand also has a trigger domain that can bind to a free-floating trigger strand and allow it to activate the robot. The trigger strand removes the inhibitor from the robot through a reversible strand displacement reaction—the trigger has no hand domain, and so, the activated robot can still interact with the trigger and inhibitor complex to reverse the reaction. If the trigger strand had a hand domain, it would pick up any cargo just like the robot can. Because we wanted to control the activation of the robot not only for random walking but also for cargo sorting, we decided to leave out the hand domain but bias the activation reaction forward by using a large excess of the trigger strand.

To make the robot stop walking at the destination, we designed a goal strand that is similar to a track strand but with both complementary foot domains. Upon reaching the goal, the robot will have no free foot to take further steps (Fig. 2C). To monitor the fraction of origami with a robot at the goal location, we labeled the 3′ end of the robot with a quencher and the 5′ end of the staple adjacent to the goal with a fluorophore. Goal locations with and without a robot should yield a low and high fluorescence state, respectively.

There were three main observations that led to our design choices and experimental procedures for successfully making the robot perform a random walk: (i) The rigidity of DNA origami as a testing ground for the robot affects the undesired reactions; (ii) the DNA sequence of the foot domains of the robot affects the rate of walking; and (iii) the purity of DNA

origami affects the completion level of desired reactions.

We first used a single-layer rectangular DNA origami (*6*) to build a testing ground for the DNA robot (fig. S1A). In a negative control experiment for the random walk—the robot was placed at various distances apart from the goal, but no track was provided—we discovered that a small fraction of robots still reached the goal (fig. S1B). The more surprising observation was that the closer the robot was placed to the goal, the more substantial the undesired interaction was, despite the fact that the closest distance was already three times farther than the designed reachable distance between the robot and the goal. We expect that a goal on one origami can interact with a robot on another, but if interactions between origami were the only explanation, we would not expect any correlation between the level of interaction and the distance between the robot and goal. Thus, we hypothesized that interactions within the same origami might have also played a role in the experiment because of the structural flexibility of the single-layer origami.

We were not concerned by the interactions between origami but decided to redesign the DNA origami structure to specifically reduce the undesired interactions within origami for the following two reasons: First, interactions between origami can be reduced by decreasing the origami concentration, but interactions within origami cannot. Moreover, interactions between origami can be simply modeled as bimolecular reactions with known concentrations and rate constants, but modeling undesired interactions within origami would be difficult without understanding how the structural fluctuation of origami affects the rate of each unimolecular reaction on the origami surface, thus making it difficult to predict the behavior of random walk and cargo sorting. To resolve these issues, we designed a double-layer square DNA origami (fig. S1D). Because the DNA structure is more rigid along the direction of the helix and somewhat flexible between helices connected by crossovers, we made the helix directions of the two layers perpendicular to each other to increase the structural rigidity of the origami. With the same negative control experiment but on the surface of the double-layer origami, we observed that the fraction of robots moving to the goal did not depend on the distance between the robot and the goal (fig. S1E), indicating that the interactions within origami were significantly reduced. The difference in structural flexibility between the single- and double-layer origami is also consistent with CanDo (*32*) simulations (fig. S1, C and F).

Next, we explored two DNA sequence choices for the foot domains of the robot: One used two distinct sequences for the two feet (fig. S2A), and another used the same (fig. S2B). With an experiment wherein the robot performs a single step after being triggered, we already observed a significant rate difference between the two choices—the latter was much faster (fig. S2C). We suspect

that the faster reaction rate had little to do with the sequences being the same but was mainly caused by the weaker binding energy of the sequence near the 3′ end of the robot. In both cases, the strand displacement reactions of the robot reaching the goal are irreversible. For irreversible reactions with the same initiation toehold, the rates should be similar if the reactant molecules are free floating in solution (30). However, studies have shown that the situation could be different if the reactant molecules are tethered to fixed locations (33). With tethered molecules, it is possible that the strand displacement reaction will end with a toehold disassociation when the disassociation rate becomes faster than the rate of branch migration toward increasingly constrained geometry. Thus, the weaker the binding energy of the foot sequence near the 3′ end of the robot, the faster the disassociation rate will be.

We developed a biophysical model to better understand the mechanism of walking, taking the geometry and the elasticity of DNA (34) into consideration (note S2.3 and fig. S3). The model further suggests that (i) the entropic cost of stretching the DNA strands significantly slows down branch migration toward the DNA origami surface, when the junction of branch migration is close enough to the surface, and (ii) a small difference in the standard free energy of the DNA sequence can result in a large difference in the rate of the robot taking a single step. With this understanding, we decided to move forward with the weaker sequence for both feet.

What did not make sense in the one-step experiment shown in fig. S2C was that the completion level of the reactions was only about 60%. What could have prevented the robot from taking just a single step? We hypothesized that the purity of origami might have played a role: In malformed origami structures, the activated robot may still be distant from the goal. To verify this hypothesis, we explored two methods for purifying the origami and compared them with unpurified origami in an experiment where the robot walks on linear tracks of varying lengths (fig. S4, A and B). The result of centrifugal filter–purified origami (fig. S4D) was fairly similar to that of unpurified origami (fig. S4C), but the gel-purified origami yielded a much better completion level: nearly 95% (fig. S4E). It was evident from the gel and atomic force microscopy (AFM) images that centrifugal filter purification was sufficient for removing excess staples but insufficient for removing the malformed origami structures (fig. S4F). Thus, we gel-purified the origami for all later experiments.

Using the above design choices and experimental procedures, we verified the formation of a linear track on origami (Fig. 2D) and demonstrated random walking on linear tracks of lengths one through eight steps (Fig. 2E). In theory (31), the expected number of steps in a random walk, which is the hitting time from a start point to an end point on a path of length n, is n^2. Numerical analysis showed that the two-thirds completion time, which can be directly obtained from experimental data, should

be similar to the expected hitting time (note S2.5 and fig. S5). In our data, the two-thirds completion time was quadratically related to the length of the track (Fig. 2E, inset). The constant term in the fitted quadratic function was attributed to the time for activating the robot and the actual tracks being three sites wide.

We simulated the activation and random-walk reactions on tracks of width three (Fig. 2F). The rate constants of the two reactions were determined by comparing the two-thirds completion time with the experimental data. The robot walks at a rate of roughly 5 min per step with a 6-nm step size, which is similar to other autonomous DNA motors on origami (19, 35). The rate of the free-floating trigger strand interacting with the inhibited robot on the origami was roughly 100 times slower than a similar strand displacement reaction between two free-floating molecules (30) but comparable to other hybridization and strand displacement rates measured on origami surfaces (36, 37). We also simulated the negative control—the reaction of the robot on one origami interacting with the goal on another without any track. The rate of this inter-origami interaction was determined to be roughly 100 times slower than the reaction of robot activation, presumably caused by the slow diffusion rate of both reactants and the decreased probability of the molecules positioned to initiate the desired reaction during a collision event.

Cargo sorting

The second building block, cargo pickup, was directly composed, together with the random-walk building block (fig. S6A). Because the inhibitor strand covers up not only the foot domain for walking but also the hand and arm domains for cargo pickup, the same activation reaction was used to control the start of the experiment. In this setup, the robot was initially placed at the center of the DNA origami, and the origami surface was fully covered by track strands so that the robot can explore the entire 2D testing ground. Three cargos of the same type were initially located near one edge of the origami. Once activated, the robot was designed to start a random walk, pick up a cargo when it bumps into one, and continue walking while carrying the cargo. Lacking the cargo drop-off functionality, the robot should only be able to pick up exactly one cargo, while leaving the other two cargos at their initial locations. As expected, the completion level of the cargo pickup was 27%, just a little below one-third (fig. S6B). The robot was also able to pick up a second type of cargo strand labeled with a different fluorophore (fig. S6C).

Adding the cargo drop-off building block to the system requires a mechanism to protect the goal strand; otherwise, the goals will directly interact with the cargos when they are mixed together before localizing at their specified destinations on the origami surface during initial assembly (fig. S7). Designing the goal inhibitor was more challenging than designing the robot

inhibitor. Neither the hand domain nor the cargo domain should be present in the trigger strand that binds to the inhibitor: Hand and arm domains together would pick up the cargos just as the robot does, and cargo and arm domains together would pick up the cargos just as the goal does except reversibly. Thus, we used two inhibitor strands instead of one, each covering up half of the goal strand and exposing a toehold in the middle for binding to one of the designed trigger strands (Fig. 3A). Similar to the robot activation reaction, the goal activation reaction is also reversible and biased forward by a large excess of the two trigger strands. After being activated, the goal can then grab a cargo from the robot if there is a robot carrying a matching cargo at its neighboring location.

In the cargo-sorting setup, six cargos of two types were initially at unordered locations near one edge of the origami, and eight goals of the corresponding types were at two separated locations near the opposite edge (Fig. 3B). There were more goals than cargos to account for the possible situation of a missing goal strand because of imperfect formation of the origami. Again, the robot was initially placed at the center of the origami. The two types of cargos were labeled with two distinct fluorophores, but only one type of goal was labeled with a quencher. In each experiment, for one type of cargo, the fluorescence signal will decrease if it is dropped off at a correct goal location; for the other type, the signal will only decrease if it is dropped off at an incorrect location. The pair of experiments showed that both types of cargos were dropped off at their desired destinations (Fig. 3B). An 80% completion level was observed, presumably because of synthesis errors in the robot, cargo, and goal strands that inhibited the desired pickup and drop-off reactions and also the presence of imperfect origami missing a robot. Nonetheless, the robot successfully sorted two types of cargos with multiple cargos per type. In contrast, without a robot, the cargos remained at their initial locations on origami (fig. S8).

The fluorescence kinetics experiments provided a quantitative understanding of the cargo-sorting behavior in bulk, but on individual origami surfaces, are the molecules where we think they are? To address this question, we performed AFM experiments shown in Fig. 3C. The challenge of visualizing the result of cargo sorting was to distinguish double-stranded complexes of cargos at goals from single-stranded track strands, as well as from partially double-stranded goals without any cargos. However, in AFM imaging, it was not directly possible to do so; thus, we had to remove all tracks and goals without cargos from the origami surfaces. Because the goals without cargos have the complementary cargo domain exposed (Fig. 3A), we designed a goal remover strand that binds to it and displaces the goal strand away from the origami surfaces (fig. S9). Next, we used exonuclease I to remove all single-stranded extensions, including the track strands. We left the initial cargo locations as double-stranded to serve as a reference
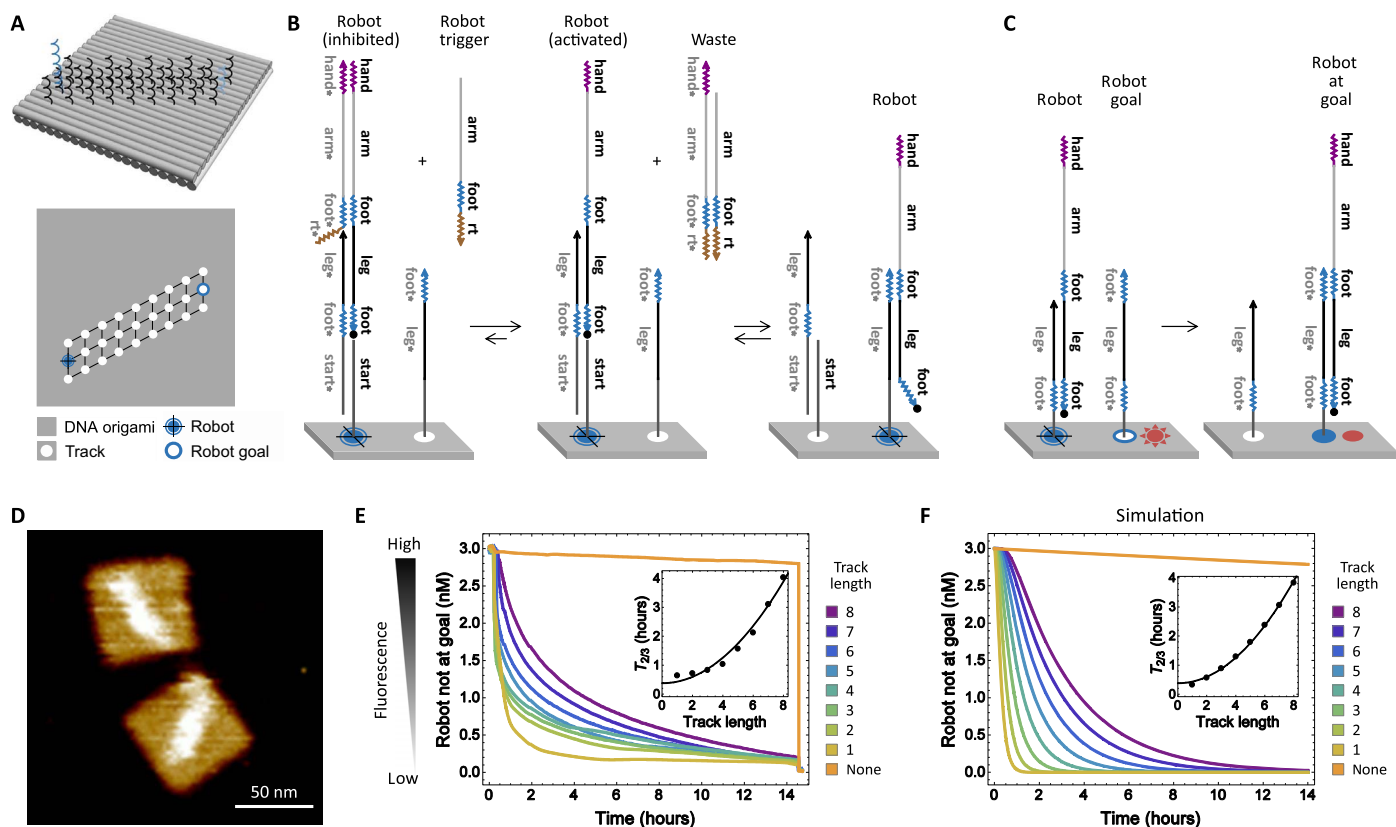
Fig. 2. The random-walk building block. (**A**) 3D and 2D schematic diagrams of an eight-step long track on a double-layer DNA origami. The lines between adjacent track locations indicate possible moves of the robot: The two types of track strands are in a checkerboard pattern, and for each step, the robot can only move between two distinct types of tracks. Thus, the hexagonal grid is functionally a square grid for the movement of the robot (fig. S4A). (**B**) Mechanism of protecting the robot from interactions with tracks and activating the robot only at the beginning of an experiment. The activation reaction is biased forward by using trigger strands at 20× higher concentration than the inhibited robot. (**C**) Mechanism of the robot reaching a goal location. (**D**) AFM image of the double-layer DNA origami with a track of length 8. (**E**) Fluorescence kinetics data of random-walk experiments with eight distinct track lengths and a negative control with no track. A 20-fold excess of free-floating robot strands, relative to the origami concentration, was added at the end of the experiments to measure the maximum possible completion level. The two-thirds completion time ($T_{2/3}$) is plotted against the track length (l). The least-squares fit of a quadratic function is $T_{2/3} = 0.38 + 0.055 \times l^2$. (**F**) Mass action simulations of the random walk and the negative control. In this model, the robot walks from an arbitrary track location to its neighboring location at $k_w = 3.5 \times 10^{-3}$ s^{-1}. The robot is initially inhibited and triggered at $k_t = 3.2 \times 10^4$ M^{-1} s^{-1}. These two rate constants were determined on the basis of the quadratic fit of the two-thirds completion time versus track length obtained from the experimental data. The negative control was simulated with the robot on one DNA origami interacting with the goal on another at $k_s = 5 \times 10^2$ M^{-1} s^{-1}.

for the orientation of the origami. In addition to being on the opposite side of the goals, these locations were also closer to the right side of the origami. In cases where the origami landed upside down on mica, we flipped the images based on the asymmetry of the initial cargo locations. Two separate AFM experiments, each with one type of cargo but both types of goals, showed that the cargos were delivered to their correct destinations (Fig. 3C and fig. S10).

To explore the parallelism of our system, we designed an experiment with two mixed populations of DNA origami in one test tube (fig. S11): one with a robot and the other without. The origami with a robot has one type of cargo labeled with a fluorophore and the other type left unmodified. The origami without a robot has the opposite labeling of cargos. With this setup, if the robot stays on the origami on which it is initially placed, the sorting of one type of cargo will be

detected but not the other. The experimental result showed that a small fraction (12 to 14%) of origami had undesired cross-talk, but mostly, the two populations of origami maintained their own identities (fig. S11).

To actually demonstrate two distinct cargo-sorting tasks taking place in parallel, we placed the robot on both populations of DNA origami but left one or the other type of goal unmodified (Fig. 4A). With this setup, if the two populations of origami maintain their own identities, the sorting of both types of cargos can be detected. Otherwise, the detected activities will be significantly reduced, because even with fluorophore-labeled cargos, delivery to the unmodified destinations cannot yield a fluorescence signal change. We did observe that the completion levels of desired reactions decreased by 16 to 18% (Fig. 4A) compared to just one population of cargo sorting (Fig. 3B). However, this decrease is still much less than 50%,

the expected completion level for the same cargos and goals interacting with each other in a well-mixed solution.

We developed a model to simulate the cargo-sorting system (Fig. 4B). The robot at any location on the track can move a single step to any immediate neighboring location at the same rate as determined in the model of the random walk (Fig. 2F), whether or not it is carrying a cargo. The robot at any location can pick up or drop off a cargo if the distance from the cargo or goal to the robot is reachable. The reachable distance is calculated on the basis of the tightest connection during the strand displacement reactions of pickup and drop-off. We assume that the maximum rates for picking up and dropping off are when the cargo or goal is an immediate neighbor of the robot, and for any further distance, the rate decreases quadratically with the distance. With the maximum rate of picking up
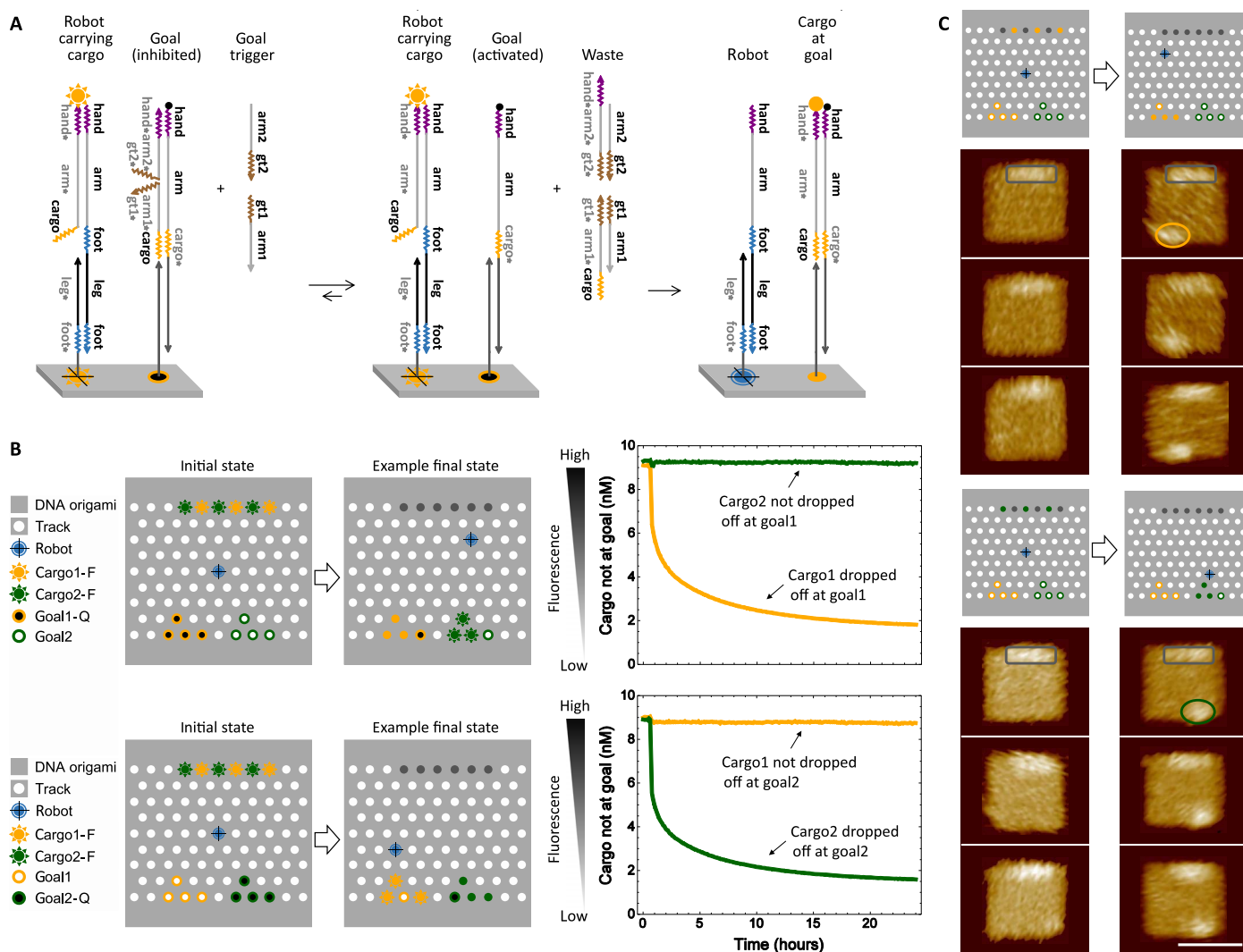
Fig. 3. Demonstration of cargo sorting. (**A**) Mechanism of protecting a goal from interactions with cargos and activating the goal only at the beginning of an experiment. The layout of the two types of tracks in all cargo-sorting systems is shown in fig. S8A. (**B**) Fluorescence kinetics data of cargo-sorting experiments with two distinct types of cargos. In the initial states, cargo1-F and cargo2-F indicate cargos labeled with fluorophores, and goal1-Q and goal2-Q indicate goals labeled with quenchers. The final states show a random choice of the locations of the robot and an unoccupied goal. (**C**) AFM images of each type of cargos at their initial locations and delivered to their goal locations, respectively. All images are at the same scale, and the scale bar in the bottom right image is 50 nm.

and dropping off being 100 times faster than the rate of walking, the simulation (Fig. 4B) semi-quantitatively reproduced the experimental data (Fig. 3B). The simulation suggested that an average of 295 steps were required for the robot to complete the cargo-sorting task.

We also analyzed the undesired inter-origami interactions, including a robot moving from one origami to another, and a robot or goal on one origami picking up a cargo on another (fig. S12A). Using a linear least-squares fit to the experimental data, we determined the completion level for each type of the modeled inter-origami interactions (fig. S12B). A robot moving between origami is the least significant (1.59%), presumably because of the high probability of interacting with local track strands and the low accessibility of densely packed track strands on another origami. A robot and goal on one origami picking up a cargo on another are both more significant (4.56 and 8.25%, respectively), likely because the cargo strands are further away from the origami surface and above the height of the track strands, and thus more accessible. The linear model and the data agree well with each other, with experimental noise of less than 3.7% (fig. S12C).

Finally, to further exploit the parallelism enabled by localization on origami, we demonstrated a single cargo-sorting task collectively performed by multiple robots (Fig. 4C). We moved the initial location of the robot away from the cargos to increase the difficulty of cargo sorting. We chose five robot locations and ranked them by how long it takes for each robot to individually sort the cargos based on simulations (fig. S13A). We increased the number of robots one at a time in each experiment, from the fastest to the slowest robot predicted by simulations. In this way, if the overall speed for cargo sorting increases with more robots, it should be a result of the collective behavior rather than any particularly fast robot. Increasing the number of robots reduced the two-thirds completion time of cargo sorting from more than 10 hours to less than 1 hour, and four robots were sufficient to accomplish the task at a near optimal speed (Fig. 4C).

An illuminating fact in the multirobot experiment is that the increasing number of robots brought up the completion level from a little below 80% to nearly 100%. This observation excluded the possibility of malfunctioning cargo or goal molecules, suggesting that either the robot itself malfunctions or a fraction of origami is missing a robot. If the probability that an individual robot malfunctions or is missing is 20%, then experiments with m robots should have a completion level of $1 - 0.2^m$, which closely agrees
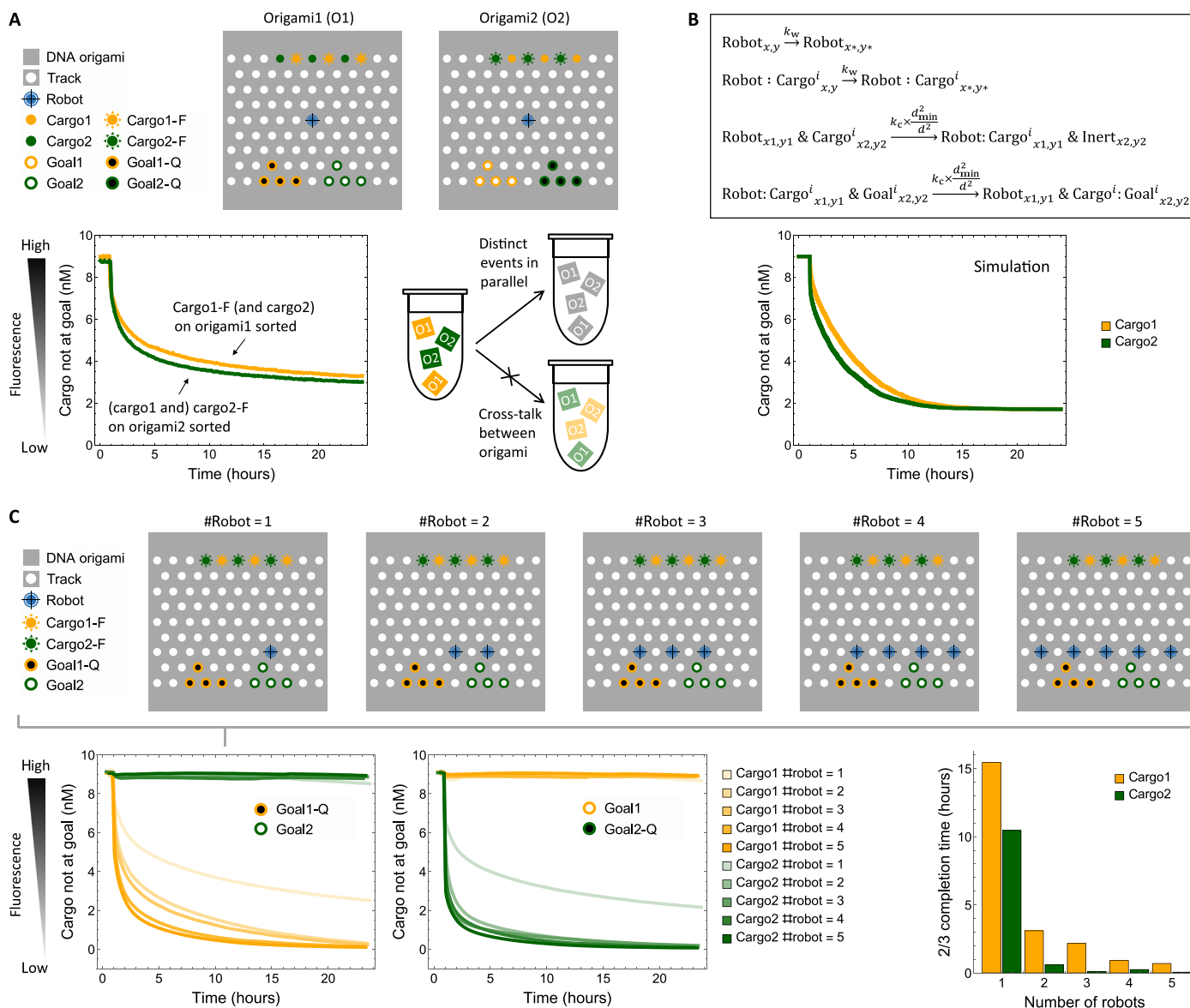
Fig. 4. Exploring the parallelism with mixed populations of DNA origami and with multiple robots on individual DNA origami surfaces. (**A**) Fluorescence kinetics experiments with two mixed populations of DNA origami, each having two types of cargos that can be sorted separately. (**B**) Stochastic simulation of sorting two types of cargos as a continuous-time Markov chain. $Robot_{x,y}$ indicates a robot at an arbitrary track location (x, y). $(x*, y*)$ is a neighboring location of (x, y). $Cargo^i$ and $Goal^i$ indicate specific types of cargo and goal, respectively. d is the Euclidean distance between (x_1, y_1) and (x_2, y_2). d_{Min} is the Euclidean distance between a robot and a cargo or goal at its immediate neighboring location. Because there are 16 base pairs (bp) between the closest staple extension locations and there is a 1-bp deletion every three staple columns for origami twist correction, d_{Min} is calculated as $(16 \times 3 - 1)/3$ bp $\times 0.34$ nm per bp = 5.33 nm. The model allows the robot to

pick up a cargo from (or drop off a cargo to) a location that is not its immediate neighbor, if the distance is within the reachable range, but the rate of the reaction decreases quadratically with the distance. Because the total number of base pairs in the double-stranded foot, leg, and cargo (or goal) attacher domains is 41 bp, and the total number of nucleotides in the single-stranded foot and linker domains is 16 nucleotides (nt), the maximum reachable distance is calculated as 41 bp $\times 0.34$ nm per bp + 16 nt $\times 0.5$ nm per nt = 21.94 nm. The rate of random walk is $k_w = 3.5 \times 10^{-3}$ s^{-1}, and the rate of closest cargo pickup and drop-off is $k_c = 100 \times k_w$. We assume that only 80% of the cargos can be successfully delivered to a goal location due to a fraction of origami missing a functional robot. This fraction was determined on the basis of the experimental data shown in Fig. 3B. (**C**) Fluorescence kinetics experiments with multiple robots collectively performing a single cargo-sorting task.

with the experimental data (Fig. 4C). We simulated the multirobot systems, assuming that each robot is present with an 80% probability. The simulations semiquantitatively captured the experimental results (fig. S13C).

Discussion

We developed a simple algorithm and three building blocks for a DNA robot that performs

cargo sorting at the molecular level. We demonstrated that the robot can explore a 2D testing ground on the surface of DNA origami, pick up multiple cargos of two types that were initially at unordered locations, and deliver them to two separate destinations. We also demonstrated two distinct cargo-sorting tasks taking place simultaneously in one test tube and multiple robots collectively performing the same task. To experimentally demonstrate the three building blocks and their composability, we tested a series of subsystems that incrementally incorporated the building block for the random walk, then the cargo pickup, and finally the cargo drop-off. Once the previous building block was successfully implemented, adding the next building block did not require any changes to previously designed components.

In principle, using exactly the same robot design, the system can be generalized in the following aspects: First, the algorithm does not require the robot to recognize the type of cargos but embeds the recognition within the destination, and thus, the system can be adapted for more than two types of cargos. Second, the algorithm allows the robot to freely explore the entire 2D testing ground, so the initial locations of the cargos can be arbitrary. Third, because the robot is designed to perform a random walk without any energy supply, sorting an increasing number of cargos should be possible. Finally, because the sorting takes place on individual origami surfaces, the parallelism can be exploited to scale up the system to perform many instances of distinct tasks, and each task can be assigned a distinct number of robots depending on the difficulty of the task.

With effort, the following aspects of the robot could be further developed. First, the robot is roughly 100,000 times slower than the fastest kinesin motor ([38]). From our understanding of how the DNA sequence of the foot domains affects the rate of walking, we believe that it is possible to increase the rate by at least 100 times by adding single-stranded tails to increase the initiation rate of localized strand displacement reactions and by using sequences with weaker binding energy (fig. S3B). It may also be possible to further increase the rate by using enzymes to drive a DNA robot ([39]) or using protein motors programmed by DNA ([40]). Second, using larger and more diverse testing grounds, such as random DNA origami arrays ([41]), could help us gain an understanding for improving the robustness of the robot. Third, using aptamers ([42]) or direct conjugation, small chemicals, metal nanoparticles, and proteins can be transported as cargo molecules so that cargo sorting could be used for chemical synthesis ([21, 43, 44]) and fabrication of molecular devices ([45, 46]). For example, in chemical synthesis, desired products can only be assembled if the chemical groups are linked together in the right order. Thus, cargo-sorting robots could work together with the assembly robots to allow the synthesis of desired products from components that are originally randomly distributed. In molecular devices, cargo-sorting robots could be triggered to rearrange circuit components, such as nanoparticles, so that the function of the device can be adaptive to environmental signals. Finally, making molecular robots work in biological environments could lead to programmable therapeutics ([47, 48]). For example, microRNA involved in diseases could be programmed as triggering signals for cargo-sorting tasks that gather protein subunits together to function as drugs.

More generally, our interest is in developing simple algorithms and modular building blocks that will eventually be used for systematic construction of molecular robots that can perform a variety of tasks. We believe the three building blocks that we developed here are not limited to the cargo-sorting task alone. For example, inspired by ant foraging ([5]), adding a new building block

for leaving pheromone-like signals on a path, DNA robots could be programmed to find the shortest path and efficiently transport cargo molecules. With simple communication between the robots ([49]), they could perform even more sophisticated tasks. Similar to how DNA strand displacement reactions on origami surfaces can be used to construct arbitrary logic circuits ([50]) and chemical reaction networks ([51]), it should be possible to generalize a small set of DNA strand displacement building blocks, including those shown in this work, to perform arbitrary mechanical tasks defined within a certain framework ([1]). With systematic approaches, molecular robots could be easily programmed like macroscopic robots, but working in microscopic environments.

Materials and methods
DNA oligonucleotide synthesis

DNA oligonucleotides were purchased from Integrated DNA Technologies (IDT). The regular staples, track staples and trigger strands were purchased unpurified (standard desalting). The robot, cargo and goal strands, the inhibitor strands, and the staples with extensions for localizing robot, cargos and goals (referred to as robot start, cargo and goal staples, respectively) were purchased purified (HPLC). All strands were purchased at 100 μM in TE buffer, pH 8.0, and stored at 4°C.

Annealing protocol and buffer condition

DNA origami was annealed with 30 nM M13 scaffold (Bayou Biolabs) and a 10-fold excess of the regular, track, robot start, cargo and goal staples, 11-fold excess of the cargo attacher strands, and 12-fold excess of the cargo strands in 1× TAE buffer with 12.5 mM Mg^{2+}. The buffer was prepared from 50× TAE, pH 8.0 (Fisher BioReagents) and magnesium acetate tetrahydrate (Fisher BioReagents). The inhibited robot and goal complexes were annealed at 20 μM with a 20% excess of the inhibitor strands. Annealing was performed in a thermal cycler (Eppendorf), first heating up to 90°C for 5 min, and then slowly cooling down to 20°C at the rate of 6 s per 0.1°C.

Purification

After annealing, the DNA origami sample was loaded on a 2% agarose gel, run on ice for 2 hours at 80 V in 1× TAE/Mg^{2+} buffer. The appropriate bands were then cut out from the gel and purified using the Freeze 'N Squeeze DNA gel extraction spin columns (Biorad). The inhibited robot and goal complexes were purified using 15% polyacrylamide gel electrophoresis (PAGE). After incubating the DNA origami with an approximately 2-fold excess of the inhibited robot and goal complexes for 5 hours at room temperature, the sample was purified three times using 0.5 mL and 100 KDa spin filters (Amicon, #UFC510096), each time for 12 min at 2,500 Relative Centrifugal Force (RCF).

DNA origami concentration measurement

The concentration of DNA origami with the robot, tracks, cargos and goals was measured in a

spectrofluorimeter (Fluorolog-3, Horiba), using the fluorescence signal of an embedded staple labeled with a ROX fluorophore, and comparing the signal with a calibration curve (i.e., a linear fit of the measurements of raw fluorescence levels at varying concentrations) of the fluorophore-labeled strand by itself.

Fluorescence spectroscopy

Fluorescence kinetics data were collected every 2 min in a spectrofluorimeter (Fluorolog-3, Horiba). Experiments were performed with 50 μL reaction mixture per cuvette, in fluorescence cuvettes (Hellma #105.251-QS) at 25°C. The excitation/emission wavelengths were set to 534/554 nm for ATTO 532 and 602/624 nm for ATTO 590. Both excitation and emission bandwidths were set to 5 nm, and the integration time was 10 s for all experiments. Samples for fluorescence spectroscopy were diluted to 3 nM of the origami concentration. Baseline measurements of the samples were taken for 30 min. A 20-fold excess of the trigger strands was then added. To measure the maximum possible completion level at the end of each experiment, a 20-fold excess of free-floating robot strands with and without quenchers was added in random-walk and cargo-pickup experiments, respectively; a 20-fold excess of free-floating goal strands with quenchers was added in cargo-sorting experiments.

Atomic force microscopy

Samples for AFM imaging were prepared by diluting the origami to 1 nM in 1× TAE/Mg^{2+} buffer. After dilution, 40 μL of the sample was deposited onto freshly cleaved mica (SPI Supplies, 9.5 mm diameter, #01873-CA). After 3 minutes, the solution was removed and 40 μL of 1× TE/Mg^{2+} buffer was added onto the mica, then the sample was imaged. Samples of cargo-sorting experiments were first incubated with a 20-fold excess of goal remover strands for one hour at room temperature, and then incubated with 10 units per μL of exonuclease I (New England Biolabs #M0293S) for 18 hours at 25°C before imaging. AFM images were taken in tapping mode in fluid on a Dimension FastScan Bio (Bruker) using FastScan-D probes (Bruker). All images were scanned at a resolution of 1024 lines with 1024 pixels per line.

REFERENCES AND NOTES

1. M. Yim et al., Modular self-reconfigurable robot systems. IEEE Robot. Auto. Mag. **14**, 43–52 (2007). doi: 10.1109/MRA.2007.339623
2. M. Nakamura et al., Remote control of myosin and kinesin motors using light-activated gearshifting. Nat. Nanotechnol. **9**, 693–697 (2014). doi: 10.1038/nnano.2014.147; pmid: 25086603
3. A. Furuta et al., Creating biomolecular motors based on dynein and actin-binding proteins. Nat. Nanotechnol. **12**, 233–237 (2017). doi: 10.1038/nnano.2016.238; pmid: 27842063
4. T. Neary, D. Woods, The complexity of small universal Turing machines: A survey, in SOFSEM 2012: Theory and Practice of Computer Science, M. Bieliková, G. Friedrich, G. Gottlob, S. Katzenbeisser, G. Turán, Eds. (Springer, 2012), vol. 7147, pp. 385–405.
5. E. Bonabeau, M. Dorigo, G. Theraulaz, Inspiration for optimization from social insect behaviour. Nature **406**, 39–42 (2000). doi: 10.1038/35017500; pmid: 10894532

6. P. W. K. Rothemund, Folding DNA to create nanoscale shapes and patterns. *Nature* **440**, 297–302 (2006). doi: 10.1038/nature04586; pmid: 16541064

7. N. C. Seeman, Nucleic acid junctions and lattices. *J. Theor. Biol.* **99**, 237–247 (1982). doi: 10.1016/0022-5193(82)90002-9; pmid: 6188926

8. B. Yurke, A. J. Turberfield, A. P. Mills Jr., F. C. Simmel, J. L. Neumann, A DNA-fuelled molecular machine made of DNA. *Nature* **406**, 605–608 (2000). doi: 10.1038/35020524; pmid: 10949296

9. S. Venkataraman, R. M. Dirks, P. W. K. Rothemund, E. Winfree, N. A. Pierce, An autonomous polymerization motor powered by DNA hybridization. *Nat. Nanotechnol.* **2**, 490–494 (2007). doi: 10.1038/nnano.2007.225; pmid: 18654346

10. P. Ketterer, E. M. Willner, H. Dietz, Nanoscale rotary apparatus formed from tight-fitting 3D DNA components. *Sci. Adv.* **2**, e1501209 (2016). doi: 10.1126/sciadv.1501209; pmid: 26989778

11. W. B. Sherman, N. C. Seeman, A precisely controlled DNA biped walking device. *Nano Lett.* **4**, 1203–1207 (2004). doi: 10.1021/nl049527q

12. J.-S. Shin, N. A. Pierce, A synthetic DNA walker for molecular transport. *J. Am. Chem. Soc.* **126**, 10834–10835 (2004). doi: 10.1021/ja047543j; pmid: 15339155

13. P. Yin, H. Yan, X. G. Daniell, A. J. Turberfield, J. H. Reif, A unidirectional DNA walker that moves autonomously along a track. *Angew. Chem. Int. Ed.* **43**, 4906–4911 (2004). doi: 10.1002/anie.200460522; pmid: 15372637

14. J. Bath, S. J. Green, A. J. Turberfield, A free-running DNA motor powered by a nicking enzyme. *Angew. Chem. Int. Ed.* **117**, 4432–4435 (2005). doi: 10.1002/ange.200501262

15. Y. Tian, Y. He, Y. Chen, P. Yin, C. Mao, A DNAzyme that walks processively and autonomously along a one-dimensional track. *Angew. Chem. Int. Ed.* **44**, 4355–4358 (2005). doi: 10.1002/anie.200500703; pmid: 15945114

16. R. Pei *et al.*, Behavior of polycatalytic assemblies in a substrate-displaying matrix. *J. Am. Chem. Soc.* **128**, 12693–12699 (2006). doi: 10.1021/ja058394n; pmid: 17002363

17. P. Yin, H. M. T. Choi, C. R. Calvert, N. A. Pierce, Programming biomolecular self-assembly pathways. *Nature* **451**, 318–322 (2008). doi: 10.1038/nature06451; pmid: 18202654

18. T. Omabegho, R. Sha, N. C. Seeman, A bipedal DNA Brownian motor with coordinated legs. *Science* **324**, 67–71 (2009). doi: 10.1126/science.1170336; pmid: 19342582

19. K. Lund *et al.*, Molecular robots guided by prescriptive landscapes. *Nature* **465**, 206–210 (2010). doi: 10.1038/nature09012; pmid: 20463735

20. S. F. J. Wickham *et al.*, A DNA-based molecular motor that can navigate a network of tracks. *Nat. Nanotechnol.* **7**, 169–173 (2012). doi: 10.1038/nnano.2011.253; pmid: 22266636

21. H. Gu, J. Chao, S.-J. Xiao, N. C. Seeman, A proximity-based programmable DNA nanoscale assembly line. *Nature* **465**, 202–205 (2010). doi: 10.1038/nature09026; pmid: 20463734

22. C. Jung, P. B. Allen, A. D. Ellington, A stochastic DNA walker that traverses a microparticle surface. *Nat. Nanotechnol.* **11**, 157–163 (2016). doi: 10.1038/nnano.2015.246; pmid: 26524397

23. M. Bentley, G. Banker, The cellular mechanisms that maintain neuronal polarity. *Nat. Rev. Neurosci.* **17**, 611–622 (2016). doi: 10.1038/nrn.2016.100; pmid: 27511065

24. N. R. Franks, A. B. Sendova-Franks, Brood sorting by ants: Distributing the workload over the work-surface. *Behav. Ecol. Sociobiol.* **30**, 109–123 (1992). doi: 10.1007/BF00173947

25. D. E. Knuth, *The Art of Computer Programming: Sorting and Searching* (Pearson Education, 1998), vol. 3.

26. S. Artavanis-Tsakonas, M. D. Rand, R. J. Lake, Notch signaling: Cell fate control and signal integration in development. *Science* **284**, 770–776 (1999). doi: 10.1126/science.284.5415.770; pmid: 10221902

27. J.-L. Deneubourg *et al.*, The dynamics of collective sorting robot-like ants and ant-like robots, in *From Animals to Animats: Proceedings of the First International Conference on Simulation of Adaptive Behavior*, J.-A. Meyer, S. W. Wilson, Eds. (MIT Press, 1991), pp. 356–363.

28. O. Holland, C. Melhuish, Stigmergy, self-organization, and sorting in collective robotics. *Artif. Life* **5**, 173–202 (1999). doi: 10.1162/106454699568737; pmid: 10633575

29. A. J. Turberfield *et al.*, DNA fuel for free-running nanomachines. *Phys. Rev. Lett.* **90**, 118102 (2003). doi: 10.1103/PhysRevLett.90.118102; pmid: 12688969

30. D. Y. Zhang, E. Winfree, Control of DNA strand displacement kinetics using toehold exchange. *J. Am. Chem. Soc.* **131**, 17303–17314 (2009). doi: 10.1021/ja906987s; pmid: 19894722

31. L. Lovász, Random walks on graphs: A survey. *Combinatorics* **2**, 1–46 (1993).

32. C. E. Castro *et al.*, A primer to scaffolded DNA origami. *Nat. Methods* **8**, 221–229 (2011). doi: 10.1038/nmeth.1570; pmid: 21358626

33. P. Šulc, T. E. Ouldridge, F. Romano, J. P. K. Doye, A. A. Louis, Simulating a burnt-bridges DNA motor with a coarse-grained DNA model. *Nat. Comput.* **13**, 535–547 (2014). doi: 10.1007/s11047-013-9391-8

34. S. B. Smith, Y. Cui, C. Bustamante, Overstretching B-DNA: The elastic response of individual double-stranded and single-stranded DNA molecules. *Science* **271**, 795–799 (1996). doi: 10.1126/science.271.5250.795; pmid: 8628994

35. S. F. J. Wickham *et al.*, Direct observation of stepwise movement of a synthetic molecular transporter. *Nat. Nanotechnol.* **6**, 166–169 (2011). doi: 10.1038/nnano.2010.284; pmid: 21297627

36. A. Johnson-Buck, J. Nangreave, S. Jiang, H. Yan, N. G. Walter, Multifactorial modulation of binding and dissociation kinetics on two-dimensional DNA nanostructures. *Nano Lett.* **13**, 2754–2759 (2013). doi: 10.1021/nl400976s; pmid: 23701430

37. M. Teichmann, E. Kopperger, F. C. Simmel, Robustness of localized DNA strand displacement cascades. *ACS Nano* **8**, 8487–8496 (2014). doi: 10.1021/nn503073p; pmid: 25089925

38. N. Hirokawa, Y. Noda, Y. Tanaka, S. Niwa, Kinesin superfamily motor proteins and intracellular transport. *Nat. Rev. Mol. Cell Biol.* **10**, 682–696 (2009). doi: 10.1038/nrm2774; pmid: 19773780

39. K. Yehl *et al.*, High-speed DNA-based rolling motors powered by RNase H. *Nat. Nanotechnol.* **11**, 184–190 (2016). doi: 10.1038/nnano.2015.259; pmid: 26619152

40. A. J. M. Wollman, C. Sanchez-Cano, H. M. J. Carstairs, R. A. Cross, A. J. Turberfield, Transport and self-organization across different length scales powered by motor proteins and programmed by DNA. *Nat. Nanotechnol.* **9**, 44–47 (2014). doi: 10.1038/nnano.2013.230; pmid: 24213281

41. G. Tikhomirov, P. Petersen, L. Qian, Programmable disorder in random DNA tilings. *Nat. Nanotechnol.* **12**, 251–259 (2017). doi: 10.1038/nnano.2016.256; pmid: 27893729

42. R. A. Muscat, J. Bath, A. J. Turberfield, Small molecule signals that direct the route of a molecular cargo. *Small* **8**, 3593–3597 (2012). doi: 10.1002/smll.201201055; pmid: 22893622

43. Y. He, D. R. Liu, Autonomous multistep organic synthesis in a single isothermal solution mediated by a DNA walker. *Nat. Nanotechnol.* **5**, 778–782 (2010). doi: 10.1038/nnano.2010.190; pmid: 20935654

44. W. Meng *et al.*, An autonomous molecular assembler for programmable chemical synthesis. *Nat. Chem.* **8**, 542–548 (2016). doi: 10.1038/nchem.2495; pmid: 27219697

45. T.-G. Cha *et al.*, A synthetic DNA motor that transports nanoparticles along carbon nanotubes. *Nat. Nanotechnol.* **9**, 39–43 (2014). doi: 10.1038/nnano.2013.257; pmid: 24317284

46. A. Kuzyk *et al.*, A light-driven three-dimensional plasmonic nanosystem that translates molecular motion into reversible chiroptical function. *Nat. Commun.* **7**, 10591 (2016). doi: 10.1038/ncomms10591; pmid: 26830310

47. S. M. Douglas, I. Bachelet, G. M. Church, A logic-gated nanorobot for targeted transport of molecular payloads. *Science* **335**, 831–834 (2012). doi: 10.1126/science.1214081; pmid: 22344439

48. H. Peng, X.-F. Li, H. Zhang, X. C. Le, A microRNA-initiated DNAzyme motor operating in living cells. *Nat. Commun.* **8**, 14378 (2017). doi: 10.1038/ncomms14378; pmid: 28262725

49. M. Rubenstein, A. Cornejo, R. Nagpal, Programmable self-assembly in a thousand-robot swarm. *Science* **345**, 795–799 (2014). doi: 10.1126/science.1254295; pmid: 25124435

50. G. Chatterjee, N. Dalchau, R. A. Muscat, A. Phillips, G. Seelig, A spatially localized architecture for fast and modular DNA computing. *Nat. Nanotechnol.* (2017). doi: 10.1038/nnano.2017.127; pmid: 28737747

51. L. Qian, E. Winfree, Parallel and scalable computation and spatial dynamics with DNA-based chemical reaction networks on a surface. *Lecture Notes Comput. Sci.* **8727**, 114–131 (2014). doi: 10.1007/978-3-319-11295-4_8

Science

A cargo-sorting DNA robot

Anupama J. Thubagere, Wei Li, Robert F. Johnson, Zibo Chen, Shayan Doroudi, Yae Lim Lee, Gregory Izatt, Sarah Wittman,
Niranjan Srinivas, Damien Woods, Erik Winfree and Lulu Qian

Sorting molecules with DNA robots
Single-stranded DNA robots can move over the surface of a DNA origami sheet and sort molecular cargoes.
Thubagere *et al.* developed a simple algorithm for recognizing two types of molecular cargoes and their drop-off
destinations on the surface (see the Perspective by Reif). The DNA robot, which has three modular functional domains,
repeatedly picks up the two types of molecules and then places them at their target destinations. No additional power is
required because the DNA robot does this by random walking across the origami surface.
Science, this issue p. eaan6558; see also p. 1095

ARTICLE TOOLS	http://science.sciencemag.org/content/357/6356/eaan6558
SUPPLEMENTARY MATERIALS	http://science.sciencemag.org/content/suppl/2017/09/14/357.6356.eaan6558.DC1
RELATED CONTENT	http://science.sciencemag.org/content/sci/357/6356/1095.full file:/content
REFERENCES	This article cites 53 articles, 7 of which you can access for free http://science.sciencemag.org/content/357/6356/eaan6558#BIBL
PERMISSIONS	http://www.sciencemag.org/help/reprints-and-permissions